Light gyroplane empennage design considerations

S. S. Houston
stewart.houston@glasgow.ac.uk
Aerospace Sciences Research Division
University of Glasgow
Glasgow, UK

ABSTRACT

The light gyroplane is a class of aircraft popular with amateur constructors and pilots. As a result, there is limited design guidance available since formal technical resources are not available to the community. Rule-of-thumb, intuition and historical experience tend to influence design evolution. Empennage configuration is a prime example of this paradigm, and the objective of this Paper is to explore those factors that influence horizontal stabiliser effectiveness with particular reference to dynamic stability. An individual-blade rotorcraft mathematical model is coupled with a vorticity-based flowfield code, necessary to capture the highly interactional aerodynamics associated with empennage location at the rear of the airframe. A parametric study of horizontal stabiliser location shows that maximum benefit from the energising influence of the propeller slipstream is obtained if the surface is placed near the edge of the propeller wake. Further, traditional design parameters such as tail volume ratio offer an incomplete indicator of empennage effectiveness without consideration of airframe blockage and propeller slipstream. It is concluded that empennage sizing calculations can be straightforward, but require due consideration of the impact of the close-coupled nature of the vehicle on stabilising surface aerodynamic effectiveness.

NOMENCLATURE

a	blade lift-curve slope, 1/rad
a_x^{hinge}, a_z^{hinge}	hinge acceleration components, m/s^2
$\overline{h}$	distance of rotor above c.g., normalised by R
$I_{flap}, I_{pitch}, I_{lag}$	blade moments of inertia, Nm^2
$\overline{l}$	distance of rotor behind c.g., normalised by R
M_u	pitch moment change with respect to perturbation in u, 1/(ms)
M_w	pitch moment change with respect to perturbation in w, 1/(ms)
M_q	pitch moment change with respect to perturbation in q, 1/s
M_Ω	pitch moment change with respect to perturbation in Ω, 1/s
$M_{w_{fuse}}$	fuselage contribution to M_w, 1/(ms)
$M_{w_{rotor}}$	rotor contribution to M_w, 1/(ms)
$M_{w_{tail}}$	tailplane contribution to M_w, 1/(ms)
$M^{bl}_{flap}, M^{bl}_{pitch}, M^{bl}_{lag}$	blade flap, feather and lag moments, Nm
m^{bl}	blade mass, kg
R	rotor radius, m
S_t	tailplane area, m^2
t_c	rotor thrust coefficient
u	velocity perturbation along Ox body axis, ms^{-1}
w	velocity perturbation along Oz body axis, ms^{-1}
q	pitch rate, rad/s; free-stream dynamic pressure, Pa
q_p	dynamic pressure at tailplane due to propeller slipstream, Pa
q_s	dynamic pressure at tailplane, Pa
$\underline{u}$	control vector
$\underline{x}$	state vector

Paper No. 3648. Manuscript received 12 November 2010, revised version received 18 March 2011, accepted 31 March 2011.

y_{cg}^{bl} distance of blade c.g. from hinge, m
V equivalent airspeed, ms^{-1}
V_t tailplane volume ratio
Z force along aircraft z-body axis, N
α angle-of-attack, rad
β_{1c} rotor disc longitudinal flap angle, rad
η_s longitudinal rotor tilt angle, rad
μ rotor tip speed ratio
ρ air density, kg/m^3
υ flow velocity, ms^{-1}
Ω rotorspeed; rotorspeed perturbation, rad/s
ω flow vorticity, 1/s
$\omega_x^{bl},\omega_y^{bl},\omega_z^{bl}$ blade angular velocities in blade axes, rad/s
‘ denotes normalised derivative

1.0 INTRODUCTION

Most aircraft, contemporary and historical, have empennage assemblies that mount vertical and horizontal surfaces. They are present to confer a degree of natural stability and as a means of mounting moveable surfaces for pitch and yaw control. Design rules for fixed-wing aircraft embrace sizing and effectiveness of the tailplane as an integral element of a process for conferring static, manoeuvre and dynamic stability, and the tail volume ratio is a key parameter in this regard[1]. While early helicopter analyses emulated such fixed-wing practice[2], the use of horizontal stabilisers on helicopters is driven largely by the simple requirement to tailor the characteristics of an aerodynamically unstable fuselage[3]. However the intrinsic difference between helicopter and aeroplane pitch dynamic stability has a subtler interpretation – the aeroplane wing/cg relationship determines pitch stiffness, while the tailplane provides damping. Conversely the helicopter rotor provides pitch damping, and the tailplane confers pitch stiffness. This is of course a simplification but it does capture the essential distinction. Further, since the helicopter rotor integrates the functions of lift, control and propulsion the stabiliser is normally fixed as there is usually no requirement for a control function other than in particular cases, e.g. Refs 3-5. The helicopter aerodynamicist does have one specialised application for a horizontal tailplane that his fixed-wing counterpart does not have to consider, and that is to provide an airframe pitch moment in cruise that minimises flapping and hence shaft bending[5]. Whatever the engineering driver behind tailplane design, the helicopter application usually presents a range of complications due to the aerodynamic interactions between rotor wakes and airframe. These include pitch-up at low speed during transition to forward flight[5], and pitch coupling with sideslip[6].

The literature appears to contain no guidance for gyroplane tailplane design other than Ref. 7 which proposes a tail volume ratio of between 0·12 and 0·15, appropriate for the tractor configuration with relatively long fuselage. This is quite dissimilar to the close-coupled, pusher propeller configuration of contemporary machines. The objective of this Paper is therefore to examine the effectiveness of tailplanes for modern gyroplane configurations. The primary aim is to determine sizing design guidelines in the context of the unique and complex interactional aerodynamic environment behind the aircraft.

2.0 BACKGROUND

The light gyroplane is an attractive machine for the amateur or sport pilot as it is intrinsically a mechanically simple and compact configuration. Primarily homebuilt either from personal design, plans or kits these aircraft are easy to store and maintain and therefore possess all the hallmarks of low-cost personal aviation. The majority utilise a configuration established by Bensen in the 1950s[8] that comprised an open airframe driven by a pusher propeller and supported by a two-bladed teetering or ‘see-saw’ rotor system with no cyclic or collective pitch – pitch and roll control is effected by tilting the rotor head. The technical literature is however sparse after 1937 when NACA appeared to cease research on gyroplanes[9]. A comprehensive program of research was started in 1991 following a spate of fatal accidents in the UK and this generated a range of modelling, wind tunnel and flight test activities[10-13] which was in part designed to contribute to a formal, national airworthiness design standard[14]. This work identified the significance of the vertical location of the centre of gravity in relation to the propeller thrust line for static and dynamic stability across the speed range. The role of a horizontal tailplane was more ambiguous, and this is at variance with hearsay evidence in the gyroplane community. Light gyroplanes typically have featured at best vestigial surfaces (see Fig. 1), although most current machines now sport large tailplanes (see Fig. 2). Some enthusiasts have sought to optimise the location of the tailplane in the propeller slipstream[15] in an attempt to improve effectiveness, particularly at low speed. Others have explored pitch control augmentation using tail-mounted elevators[16]. Perhaps there is tacit acceptance that the empennage does not contribute to dynamic stability as much as engineering intuition might suggest. Wind-tunnel testing of the configuration shown in Fig. 2 indicates that a horizontal tailplane can alter airframe aerodynamic characteristics, but questions the effectiveness of even a large surface[11].

Engineering intuition suggests that the configuration of the aircraft is such that interactional aerodynamic phenomena may have a significant role to play in the effectiveness of a horizontal stabiliser. Helicopter flight mechanics models typically take an empirical approach to implementation of main rotor wake and empennage impingement[17] which

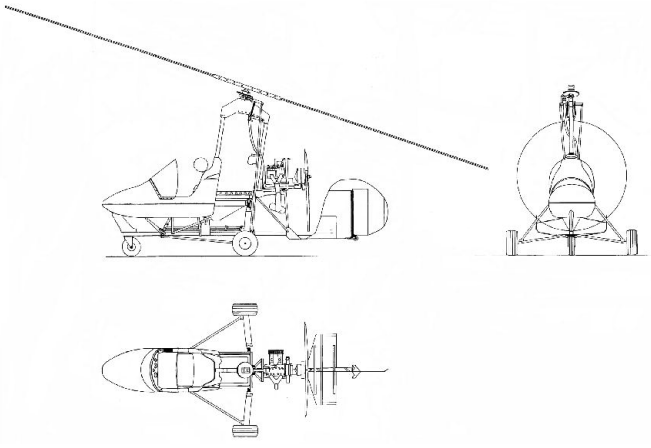

Figure 1. General arrangement of the Montgomerie-Parsons two-place (Modified) Gyroplane.

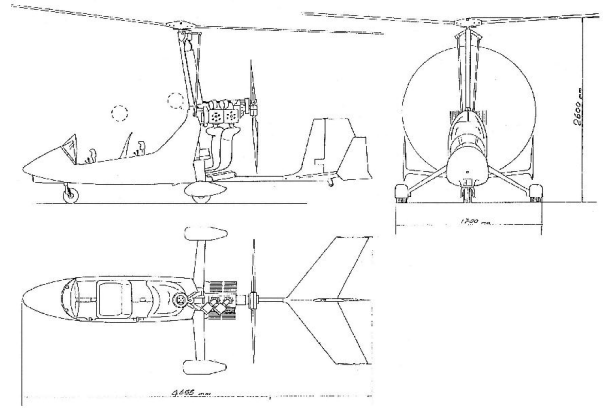

Figure 2. General arrangement of the VPM M16 Gyroplane.

https://doi.org/10.1017/S000192400000614X Published online by Cambridge University Press

sees the local angle-of-attack at the tailplane modified by a momentum theory-derived main rotor downwash term. In principle a similar approach can be adopted for the gyroplane, whereby the local dynamic pressure can by modified by superimposing propeller induced velocity on the airspeed at the tail. However, simple momentum theory may be inadequate for deriving this term without explicit knowledge of the flowfield at the tail. This can be obtained if the flight mechanics model is coupled with a vorticity transport flowfield code, Ref. 18. Previous application of this approach for a helicopter problem has been validated against flight test data[19].

3.0 MATHEMATICAL MODELLING

The implementation of the coupled rotor-fuselage model employs an individual blade-element formulation to calculate the aerodynamic and inertial loads on each blade of the gyroplane. The model has been used previously for helicopter model validation and simulation studies[20,21] and for the simulation of gyroplanes[13], although these applications used a finite-state dynamic inflow model. Replacement of this element by the vorticity-transport flowfield model[18] is described and validated elsewhere[19]. Application to autorotation problems has been limited to helicopter configurations[22]. Properties of the model are summarised in Table 1.

The individual blade motions are governed by the standard rigid-body dynamic equations[23];

$$\begin{aligned} I_{flap}(\dot{\omega}_x^{bl} + \omega_y^{bl}\omega_z^{bl}) - m^{bl} y_{cg}^{bl} a_z^{hinge} &= M_{flap}^{bl} \\ I_{pitch}(\dot{\omega}_y^{bl} - \omega_x^{bl}\omega_z^{bl}) &= M_{pitch}^{bl} \\ I_{lag}(\dot{\omega}_z^{bl} - \omega_x^{bl}\omega_y^{bl}) + m^{bl} y_{cg}^{bl} a_x^{hinge} &= M_{lag}^{bl} \end{aligned} \quad \ldots (1)$$

Where expressions for the blade angular velocities ω_x^{bl}, ω_y^{bl}, and ω_z^{bl} and the hinge acceleration terms α_x^{hinge} and α_z^{hinge} are derived using standard kinematic principles[20]. The applied moments M_{flap}^{bl} and M_{lag}^{bl} include spring restraint terms if appropriate, and the lag degree of freedom embodies a linear lag damper. The aerodynamic and inertial loads are transferred to the airframe via appropriate transformation to airframe-fixed hub co-ordinates following summation over blade elements (Ref. 20). The equations of motion of the airframe are written in standard state-vector form;

$$\dot{\underline{x}} = f(\underline{x}, \underline{u}) \quad \ldots (2)$$

where $\underline{x}$ contains the airframe translational and angular velocity, blade flap, lag and feather angles and rates for each blade on each rotor, the angular velocity of each rotor and engine torques. The control vector $\underline{u}$ is aircraft configuration-specific: for conventional single main and tail rotor helicopters, for example, there are three main rotor controls and one tail rotor control; for the gyroplane there are two main rotor controls and rudder and propeller controls. Equation (2) is then integrated to obtain the unsteady motion of the vehicle. Trim in steady flight is achieved by successive approximation to a state in which the mean forces and moments on the airframe are zero over a period that is long compared to the main rotor's rotational period, Ref. 20. Such an approach is necessary due to the inherent periodicity of the solution. The rotor/fuselage model is therefore a very conventional yet contemporary individual blade, blade element representation of a generic two-rotor aircraft. It is rendered type-specific by data that defines blade mass distribution and aerodynamic properties, rotor hinge offset and restraint, the location and orientation of the rotors on the airframe and the airframe's mass distribution and aerodynamic characteristics.

Coupling with the vorticity transport model allows induced velocity at any point in a defined computational environment to be determined, and hence the aerodynamic environment at airframe components to be calculated. The model offers therefore a rigorous and consistent means of dealing with aerodynamic interactions. The approach, developed by Brown (Ref. 18), has found application in a range of aerodynamic studies but was initially developed to support examination of problems in flight mechanics, Ref. 19. Salient elements are summarised here.

In an incompressible flow the velocity υ anywhere in the neighbourhood of the rotorcraft is related by the Poisson equation;

$$\nabla^2 \upsilon = -\nabla \times \omega \quad \ldots (3)$$

to the vorticity $\omega = \nabla \times \upsilon$ in the flow surrounding the rotorcraft. Under the further assumption of limitingly small viscosity, the Navier-Stokes equation for the flow reduces to the unsteady vorticity-transport equation;

$$\frac{\partial}{\partial t}\omega + \upsilon \cdot \nabla\omega - \omega \cdot \nabla\upsilon = S \quad \ldots (4)$$

Table 1
Mathematical model description

Model item	Characteristics
Rotor dynamics (both rotors)	• up to 10 individually-modelled rigid blades
	• fully-coupled flap, lag and feather motion
	• blade attachment by offset hinges and springs
	• linear lag damper
Rotor loads	• aerodynamic and inertial loads represented by up to 10 elements per blade
Blade aerodynamics	• lookup tables for lift and drag as function of angle-of-attack and Mach number
Wake model	• Peters dynamic inflow model
	• uniform and harmonic components of inflow
	• Optional Brown vorticity transport model
	• full flowfield
	• rudimentary interaction with tail surfaces
	• ground effect
Transmission	• coupled rotorspeed and engine dynamics
	• up to three engines
	• geared or independently-controlled rotor torque
Airframe	• fuselage, tailplane and fin aerodynamics by lookup tables or polynomial functions
Atmosphere	• International Standard Atmosphere
	• provision for variation of sea-level temperture and pressure

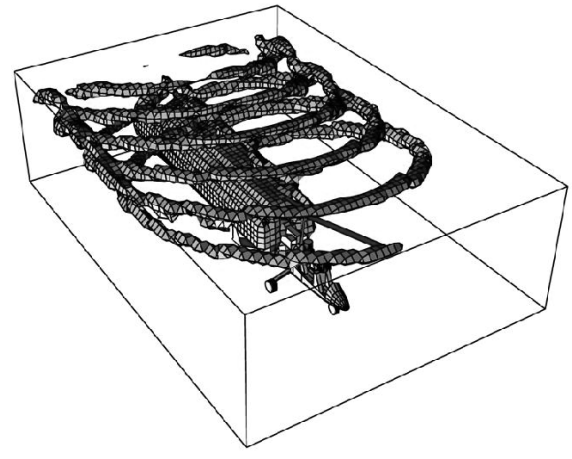

Figure 3. Calculated flowfield, VPM M16, 70mph.

https://doi.org/10.1017/S000192400000614X Published online by Cambridge University Press

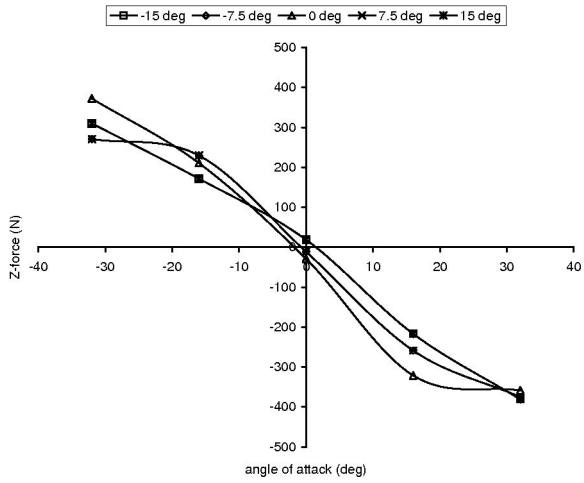

Figure 4. VPM M16 tailplane normal force variation with angle-of-attack and sideslip.

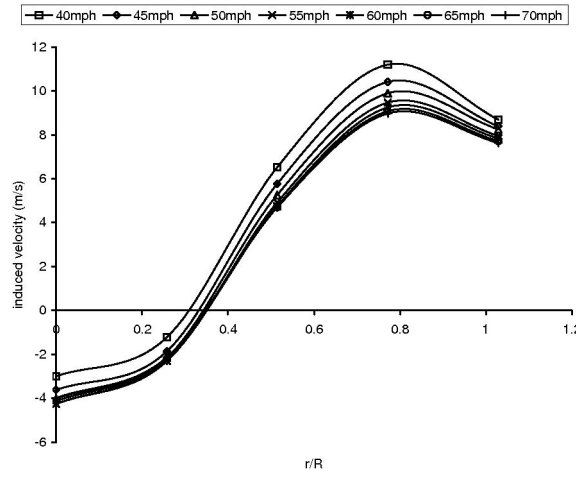

Figure 5. Induced velocity profiles at tailplane.

where the source S is a function of the aerodynamic loads on the airframe and rotors and is non-zero only where aerodynamic forces are being generated.

The grid-based algorithm for the solution of Equations (3) and (4) was developed by Brown[18]. The equations are solved numerically by tessellating the domain surrounding the aircraft into a large number of three-dimensional cells and approximating υ and ω by vector fields that are cellwise constant. Equation (3) is then solved by cyclic reduction[24], and Equation (4) is marched through time using Toro's weighted average flux (WAF) algorithm[25]. A particular advantage of the WAF algorithm is that it allows the effects of numerical diffusion of vorticity, which have plagued the accuracy of many previous attempts to construct grid-based numerical solutions of Equation (4), to be reduced to very small levels. An important feature of the present vorticity transport model is that Equation (4) is solved only after recasting in a form that specifically conserves vorticity in parts of the computational domain where the vorticity source is zero. The particular advantage of such a formulation in the context of rotorcraft flight mechanics is that there then exists a natural decomposition of the equations governing the fluid dynamics that can be exploited numerically to allow the computational time constraint imposed by the disparate rotor and body-wake timescales to be overcome,[18].

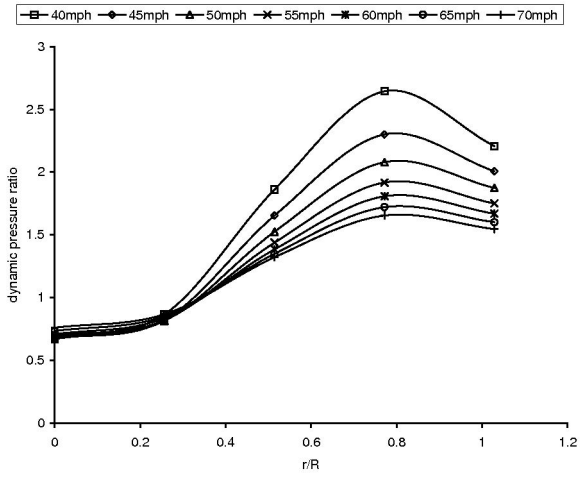

Figure 6. Dynamic pressure profiles at tailplane.

The vorticity transport model is coupled readily into the rotor-fuselage code by using the aerodynamic loads generated by the blade-element model to construct S in terms of the shed and trailed vorticity from the blades of the rotors. The velocity at each blade element of each rotor is obtained by sampling the field υ at the location of the quarter-chord of the blade element. Likewise, the field is sampled at a given location on the airframe, such as the tailplane, for calculating the loads generated by that particular component. Specific details of the numerical implementation of the vorticity transport model, and some examples verifying the predictions of the basic approach, are presented in Ref. 18. Applications of the coupled model to helicopter flight mechanics are given in Refs 19 and 22.

Figure 3 shows the calculated flowfield around the VPM M16 aircraft used in this study. The vorticity contours are plotted only above a certain value to highlight essential features in the flow, hence only the main rotor blade tip vortices are presented although the propeller wake is seen clearly. This case is for 70mph although other airspeeds show similar results.

4.0 RESULTS

4.1 Tailplane effectiveness – blockage

Figures 1 and 2 suggest the tailplane is likely to operate in an uncertain aerodynamic environment given its proximity to the pod and structure such as undercarriage. Such blockage effects are likely to reduce the dynamic pressure and hence effectiveness of the surface. Stinton[1] includes this blockage factor as a dynamic pressure ratio q_s/q. If the tailplane lift-curve slope is assumed to be a theoretical maximum of 2π, then;

Table 2
Comparison of typical fixed- and rotary-wing aircraft tailplane volume ratios

Aircraft	Tailplane volume ratio
Eurocopter Bo105	0·141
Eurocopter Puma	0·099
AgustaWestland Lynx	0·143
Airbus A320	0·875
Diamond Katana	0·620
VPM M16	0·268
Montgomerie-Parsons	0·074

https://doi.org/10.1017/S000192400000614X Published online by Cambridge University Press

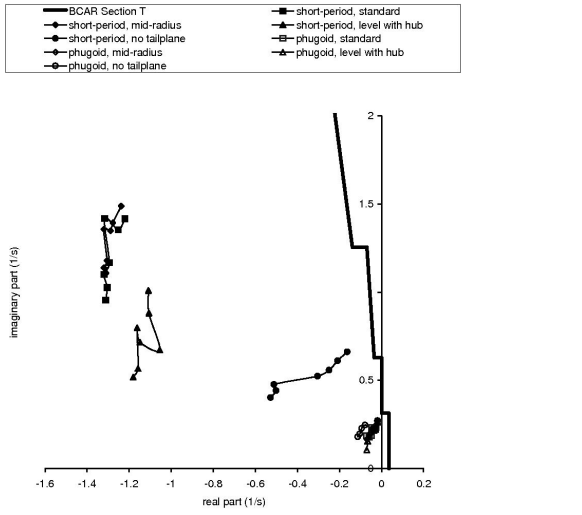

Figure 7(a). Short-period and phugoid modes; BCAR Section T compliance.

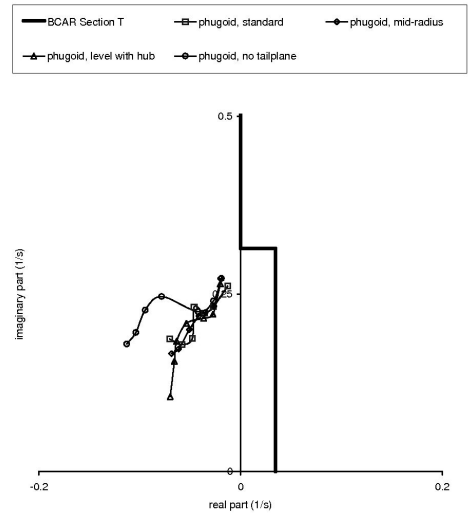

Figure 7(b). Phugoid modes; BCAR Section T compliance – expanded scale.

$$\frac{q_s}{q} = \frac{-\partial Z / \partial \alpha}{2\pi q S_t} \quad \ldots (5)$$

Figure 4 shows the variation of tailplane lift with angle-of-attack and sideslip used in the simulation model. This is a coarse form of the data presented in Ref. 11, and fails to show stall at about ±20°deg but does include the post-stall recovery and subsequent flattening of the lift profile, thus capturing the salient features of significance to the simulation of small perturbations from the majority of steady flight conditions. From the linear range, $\partial Z/\partial\alpha \approx -700 N/rad$ and since q = 574·6Pa, q_s/q = 0·215. This does not compare favourably with light aeroplane values of about 0·75[1]. Typical helicopter tailplane lift-curve slopes[26] are 3·5-3·7 rad^{-1} which is consistent with q_s/q = 0·57. Hence even the low-mounted configuration as shown in Figs 1 and 2 will suffer from relatively poor aerodynamic effectiveness. Note q_s/q = 0·215 implies that the velocity at the tailplane is about half that of the freestream.

4.2 Tailplane effectiveness – propeller slipstream

The simulation model was trimmed at a range of airspeeds between 40 and 70 mph. The induced velocity at a number of locations is shown in Fig. 5. These locations are expressed in terms of propeller radius and are above that point on the aircraft where the tailplane quarter-chord intersects the centreline. Maximum benefit from slipstream is achieved with the tailplane just inside the propeller arc. Moving further up into the propeller slipstream results in reduction of induced velocity – note that when level with the propeller hub the slipstream reverses direction and this is attributed to a strong trailed root vortex from the blades. This result is at variance with measurements reported in Ref. 15 where it is observed that while this zone exists close to the propeller, recovery takes place downstream of the propeller hub. Figure 6 presents the results in terms of the ratio of dynamic pressure at each location to the free stream value. As expected any benefit reduces with increased airspeed, with slipstream effect approximately doubling the dynamic pressure at low speed, but increasing it only by about 20-40% at high speed, whether the tailplane is located at the edge of the slipstream or half-way along propeller radius. Slipstream benefit therefore barely compensates for blockage effect, and overall the tailplane volume ratio might need to be 50 to 100% greater than helicopter values to maintain similar aerodynamic performance – indeed, this appears to be suggested by results presented in Table 2.

4.3 Static and dynamic stability

Configured with VPM M16 data, the model was trimmed and linearised across the level flight speed range with different horizontal tailplane configurations: standard aircraft; tailplane raised to a point half-way towards the level of the propeller hub; raised level with the propeller hub; and tailplane removed. Figure 7(a) shows the short-period and phugoid modes for each configuration, expressed in terms of the dynamic stability compliance boundaries of BCAR Section T. Fig. 7(b) shows the phugoid mode in expanded scale. Annotation of the points with airspeed is omitted for clarity – however it can be noted that the short-period modes increase frequency with airspeed, while the phugoid mode frequencies reduce. Some differences in phugoid characteristics are discernable in Fig. 7(b), but Fig. 7(a) puts these differences in context, showing them to be very small. Since the dynamic stability compliance requirements are predicated solely on the characteristics of the phugoid mode, the tailplane appears to have only a limited role to play in this regard. The tailplane's greatest impact is on the short-period mode. Note that tailplane location only has a pronounced effect on the short-period mode if it is raised to the level of the propeller hub, and removal of the tailplane has relatively little impact on the phugoid mode (particularly in the low to mid-speed range) but moves the short-period mode considerably, reducing damping and frequency. In fact, this mode is not a true short-period – it results from degeneration of the short-period into an aperiodic pair, and is a common and well-understood behaviour of unaugmented rotorcraft without a tailplane, Ref. 27. However, in the gyroplane case the resulting low-modulus mode then coalesces with an even lower modulus rotorspeed mode to produce the oscillation seen (the other aperiodic mode migrates rapidly to the left). Although stable and in compliance with BCAR Section T, the character of short-period longitudinal dynamics is therefore quite different from the conventional interpretation of a short-period mode.

Pitch moment stability derivative comparisons are shown in Fig. 8. All (except the tailless configuration at the higher speeds) exhibit a stabilising tendency including M_Ω, a term unique to rotorcraft in autorotation[12]. The non-monotonic appearance with speed is due to the wake model capturing flow details not normally available in rotorcraft modelling. Note that the tailplane location has a small influence on the pitch damping M_q and accounts for only about 10% of the overall value. This term is dominated by the gyroscopic precession of the rotor when a pitch rate is applied. Pitch stiffness M_w, however is changed significantly by the location of the tailplane, and its removal tends to change the sign of this derivative which is entirely responsible for the 'short-period' mode characteristic seen in Fig. 7(a).

https://doi.org/10.1017/S000192400000614X Published online by Cambridge University Press

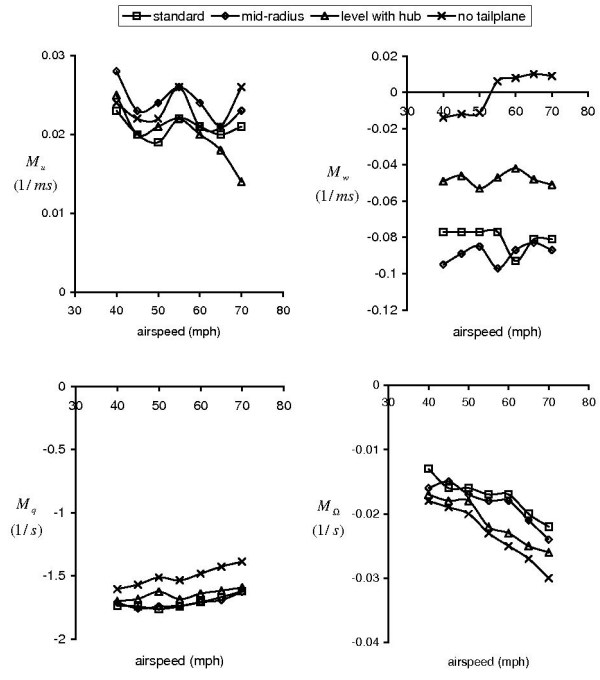

Figure 8. Pitching moment derivatives.

4.4 Determination of tail volume ratio

Parametric studies using sophisticated mathematical models of vehicle behaviour allow the engineer to converge rapidly on a design solution with a high degree of confidence. However such tools generally are not available to the amateur builder or designer of light gyroplanes, so a heuristic yet accurate means of determining tail volume ratio will allow accessible means of estimating tail size. Since simulation indicates that only the short-period mode natural frequency is sensitive to tailplane design through the angle-of-attack static stability derivative M_w, a sizing guide can be developed from;

$$M_{w_{tail}} = M_{w_{rotor}} - M_{w_{fuse}} - M_w \quad \ldots (6)$$

Incorporating the influence of both blockage and propeller slipstream effect as dynamic pressure ratios;

$$M_{w_{tail}} = -\rho V S_T \pi \left(\frac{q_s}{q}\right)\left(\frac{q_p}{q}\right)^{1/2} \quad \ldots (7)$$

Normalising and rearranging explicitly in terms of tail volume ratio;

$$\overline{V}_T = \frac{\left[M'_{w_{rotor}} + M'_{w_{fuse}} + M'_w\right]}{\mu\pi\left(\frac{q_s}{q}\right)\left(\frac{q_p}{q}\right)^{1/2}} \quad \ldots (8)$$

and following Bramwell (Ref. 17), $M'_{w_{rotor}}$ can be written;

$$\left|\phi_j\right| \quad \ldots (9)$$

$M'_{w_{fuse}}$ is calculated from wind-tunnel test data[11]. The overall angle-of-attack stability M'_w is then a matter of preference for the designer, depending primarily on the required natural frequency of the short-period mode. All other parameters are available from geometric measurement or flight test. The validity of these simple equations can be checked using simulation data, which give tail volume estimates of 0·27 and 0·23 at airspeeds of 40 and 70 mph respectively; close to the actual value of 0·268.

5.0 DISCUSSION

Positive longitudinal stability of light gyroplanes can be effected by careful placement of the propeller thrust line with respect to the centre of mass, Refs 10, 12. The UK regulator publishes advisory material emphasising this knowledge in support of compliance demonstration with the airworthiness code (Ref. 14). The role of a horizontal tailplane might therefore seem superfluous in this class of aircraft but hearsay and circumstantial evidence amongst the gyroplane community indicates that improved handling qualities can be obtained with a suitable stabiliser. It is likely, given the results here, that any tailplane augments the qualities associated with the short-period mode, rather than stabilising the phugoid mode. Even a large tailplane apparently does little for the pitch damping M_q, instead tailoring the pitch stiffness M_w. As a result, a tailplane may do little to support compliance with the requirements of the design standard but shapes the handling qualities through the pilot's perception of the short-period mode.

Given that a tailplane is to be fitted, the primary questions are associated with size and location. Equation (8) shows that tail volume ratio is inversely proportional to blockage and hence the significant blockage suggested by the wind-tunnel tests drives the requirement for a large surface, as the moment arm is by necessity very small. Since the simulation results indicate that the dynamic pressure at the tailplane can be increased by a factor of more than 2 at low speeds, it might be thought that relief from blockage effects may be obtained by placing the tailplane in the propeller wake. However, the tail volume ratio is not proportional to the inverse of the dynamic pressure recovery but its square root, diminishing any apparent numerical benefit – for example, doubling the dynamic pressure does not half the required tail size, but reduces it by 30% so that the designer may be best served by assuming $q_p/q = 1$.

6.0 CONCLUSIONS

Tail volume ratio alone is an inadequate indicator of horizontal stabiliser effectiveness for a typical light gyroplane configuration. The close-coupled nature of the aircraft means that the designer must pay due attention to relatively poor aerodynamic efficiency (or blockage) and the influence of propeller slipstream. The tailplane has a significant impact on pitch stiffness or angle-of-attack stability but contributes little to pitch damping due to the short moment arm. As a consequence the tail volume ratio can be determined exclusively by any requirement on short-period mode natural frequency. In this context the dynamic pressure recovery in the propeller slipstream is inadequate to fully compensate for blockage by the airframe.

REFERENCES

1. STINTON, D. *The Design of the Aeroplane*, BSP Professional Books, Oxford, 1983, pp 382-428.
2. BRAMWELL, A.R.S. Longitudinal Stability and Control of the Single Rotor Helicopter, Reports and Memoranda of the Aeronaut Research Council 1304, 1959.
3. PROUTY, R.W. *Helicopter Aerodynamics*, Helobooks, Mojave CA, USA, 2004, pp 375-382.
4. FERGUSON, S.W. and BUILTA, K.E. Development of a Fly-By-Wire Elevator for the Bell Helicopter Textron 214ST, American Helicopter Society 35th Annual Forum Proceedings, Washington, DC, USA, May 1979.
5. DUMOND, R.C. and SIMON, D.R. Flight investigation of design features of the S-67 winged helicopter, *J American Helicopter Society*, 1973, **18**, (3), pp 2-9.
6. AMER, K.B., PROUTY, R.W., WALTON, R.P. and ENGLE, J.E. Handling Qualities of Army/Hughes YAH-64 Advanced Attack Helicopter, American Helicopter Society 34th Annual Forum Proceedings, Washington, DC, USA, May 1978.

https://doi.org/10.1017/S000192400000614X Published online by Cambridge University Press

7. DE LA CIERVA, J. The Development of the Autogiro, *J of the Royal Aeronaut Society*, 1926, **30**, (181), pp 8-29.
8. Charnov, B.J. *From Autogiro to Gyroplane*, Praeger, Westport CT, 2003, pp 225-247.
9. WHEATLEY, J.B. An Analysis of the Factors that Determine the Periodic Twist of an Autogiro Rotor Blade, with a Comparison of Predicted and Measured Results, NACA TR600, 1937.
10. HOUSTON, S.S. Longitudinal stability of gyroplanes, *Aeronaut J*, 1996, **100**, (991), pp 1-6.
11. COTON, F., SMRCEK, L. and PATEK, Z. Aerodynamic characteristics of a gyroplane configuration, *J Aircr*, 1998, **35**, (2), pp 274-279.
12. HOUSTON, S.S. Identification of autogyro longitudinal stability and control characteristics, *J Guidance*, *Control and Dynamics*, 1998, **21**, (3), pp 391-399.
13. HOUSTON, S.S. Validation of a rotorcraft mathematical model for autogyro simulation, *J Aircr*, 2000, **37**, (3), pp 403-409.
14. Anon., British Civil Airworthiness Requirements, Section T, Light Gyroplanes, Civil Aviation Authority CAP 643 Issue 3, 2003.
15. RILEY, D. What's up back there? exploring the propwash of a pusher gyro, *Rotorcraft*, March-April 2008.
16. TRAUM, M.J., CARTER, R.G., Pitch Control Benefits of Elevators for Autogyros in Low-Speed Forward Flight, AIAA Aerospace Sciences Meeting and Exhibit, Reno, Nevada, USA, 2005.
17. BRAMWELL, A.R.S. *Helicopter Dynamics*, Arnold, London, USA, 1976, pp 171-174.
18. BROWN, R.E. Rotor wake modeling for flight dynamic simulation of helicopters, *AIAA J*, 2000, **38**, (1), pp 57-63.
19. BROWN, R.E. and HOUSTON, S.S. Rotor wake modelling for helicopter flight mechanics, *J Aircr*, 2000, **37**, (4), pp 623-629.
20. HOUSTON, S.S. Validation of a non-linear individual blade rotorcraft flight dynamics model using a perturbation method, *Aeronaut J*, 1994, **98**, (977), pp 260-266.
21. HOUSTON, S.S. Validation of a blade-element helicopter model for large-amplitude manoeuvres, *Aeronaut J*, 1997, **101**, (1001), pp 1-7.
22. HOUSTON, S.S. and BROWN, R.E. Rotor wake modeling for simulation of helicopter flight mechanics in autorotation, 2003, *J Aircr*, **40**, (5), pp 938-945.
23. BRAMWELL, A.R.S. *Helicopter Dynamics*, Arnold, London, 1976, pp 1-13.
24. SCHUMANN, U. and SWEET, R.A. A direct method for the solution of Poissons equation with Neumann boundary conditions on a staggered grid of arbitrary size, *J Computational Physics*, 1976, **20**, (2), pp 171-182.
25. TORO, E.F. A Weighted Average Flux Method for Hyperbolic Conservation Laws, Proceedings of the Royal Society of London, Series A: Mathematical and Physical Sciences, 1989, **423**, (1864), pp 401-418.
26. PADFIELD, G.D. *Helicopter Flight Dynamics*, Blackwell Science, Oxford, UK, 1996, pp 260-264.
27. PADFIELD, G.D. On the use of approximate models in helicopter flight mechanics, *Vertica*, 1981, **5**, (3), pp 243-259.